JOURNAL GEOLOGICAL SOCIETY OF INDIA
Vol.80, December 2012, pp.825-835

Imaging the Debris Internal Structure and Estimating the Effect of Debris Layer on Ablation of Glacier Ice

Wu Zhen and Liu Shiyin
State Key Laboratory of Cryospheric Science, Cold and Arid Regions Environmental and Engineering Research Institute, Chinese Academy of Sciences, Lanzhou, 730000, China
Email: wuzhen@lzb.ac.cn

Abstract: This study is a comparative investigation of the debris layer and underlying ice of the Koxkar Glacier using multi-frequency GPR with antennae having different frequencies. Together with analysis of the fluctuation of the radar signal amplitude and polarity, the debris layer and underlying ice were analyzed on the basis of high-resolution GPR images. It was found that the optimal average velocity in the shallow layer (0–4 m) is 0.06 m/ns. Images obtained with different frequency antennas have different characteristics; and the performance of the 200 MHz antenna for a debris-covered glacier is the best. The interpretation of typical GPR image is validated by using FDTD numerical model. Combining the debris layer thickness and the underlying ice structure, the effect of debris layer on ablation of glacier ice and forecast of the glacier change in the aspect of thickness-thinning and glacier retreat can be estimated. This study can provide as a reference to the formation mechanisms and estimation of the ice volume of glaciers covered by debris.

Keywords: Multi-frequency ground penetrating radar, Koxkar Glacier, Debris layer, Glacier change, China.

INTRODUCTION

The dynamic response of glaciers and permafrost to climate change is a hot topic in the scientific community (Bishop et al. 1995; Buteau et al. 2004). The proportion of the debris-covered part of a glacier to the whole glacier is a major parameter in glacier retreat and thinning(Daniels, 2005). Meltwater is not only a valuable fresh water resource but plays an important role in the economic development of downstream regions in some high-altitude Asian mountain areas (Hubbard et al. 2003). In the arid area of northwest China, meltwater is the main contributor to oases-based water resources (Yafeng et al. 2000).

The debris-covered areas account for more than 60% of the ablation areas of most continental glaciers; glacier melting and runoff concentration in the debris-covered area greatly affects the meltwater volume and route. (Nakawo and Young, 1981; Mihalcea et al. 2006; Bolch et al. 2007; Chiarle et al. 2007). These debris blankets effectively insulate the underlying ice and greatly reduce rates of ablation relative to that of uncovered ice. Debris-covered glaciers are apparently less sensitive to climatic warming and commonly advance to lower altitude than adjacent bare-ice glaciers (Clark et al. 1994; Gunnar, 1959; Rana et al. 1997; Han et al. 2005).

Therefore, the debris thickness and structure of underlying ice is a key point in the study of glacier ablation. Many techniques, such as use of a high-precision global positioning system (GPS), satellite-based remote sensing data monitoring, and measurements using a lidar altimeter, have been employed to determine changes in the elevation and velocity of the ice surface (Mayne 1962; Arcone et al. 1998; Nakawo and Rana 1999; Taurisano et al. 2006). However, such techniques cannot determine the debris thickness and inner structure, whereas, ground penetrating radar (GPR) is an effective tool for obtaining such information.

As a non-invasive investigation tool, GPR has been widely applied to environmental research in cold regions to detect the structure and composition of glaciers and permafrost (Arcone et al. 1995; Murray et al. 1997; Hodson and Ferguson, 1999; Adam and Knight, 2003; Irvine-Fynn et al. 2006). When investigating mountain glaciers without debris or ice sheets, because of the low conductivity of ice and hence the slight dielectric loss, GPR can penetrate up to several hundred or even more than 1000 m (Plewes and Hubbard, 2001). As the high-frequency antenna has good vertical image resolution, it seems ideal for penetrating debris and underlying ice (Arcone, 1995; Eisen et al. 2006). However, when using a high-frequency antenna, the lower medium may be difficult to distinguish because of

the great energy losses in the upper medium, and it is difficult to investigate the spatial relationship between debris and the underlying ice, which hampers interpretation of GPR data for debris-covered areas (Moorman et al. 2003; Paul et al. 2004; Stokes et al. 2007). It is thus necessary to determine the most optimal antenna for depicting the debris thickness and structure in a field survey. However, there is little reference on this topic in the literature.

This study had the following goals. First, we present a 2008 field survey in which three antenna frequencies were used in observations of the same section of debris-covered glacier based on detailed in situ survey data and compared the advantages and disadvantages of several antenna. Second, to understand the effect of debris thickness in spatial variability of melt rate, based on GPR survey, we extract the condition of underlying ice ablation, describe the role of spatial variability in debris thickness in the spatial characteristics of ice melt and its correlated processes on a debris-covered continental glacier. Such work is necessary to understand mass-balance variation of the debris-covered continental glacier and its response to climate changes in the western part of Tian Shan.

GEOLOGICAL SETTING AND GPR SURVEY METHODS

The Koxkar glacier is located in the Xinjiang Uyghur Autonomous Region of western China and is part of western Tien Shan. The Koxkar Glacier (41°42'N–41°53'N and 79°59'E–80°10'E) (Fig.1) is regarded as a typical continental glacier (Su and Shi, 2002).

The highest point of the glacier is Mt. Koxkar (6324 m) and the terminus is at the altitude of 3020 m. The glacier is 25.1 km in length and 83.56 km^2 in total area (Han et al. 2010). The equilibrium line is at an altitude of 4300 m. The supraglacial debris area is 19.5 km^2, which covers about 83% of the total ablation area. The surface of the debris layer is composed chiefly of clay, gray and dark-gray granite particulate fragments and rock masses. From the view of the thickness distribution, the debris layer gradually thickens with decreasing elevation in the ablation area, having an

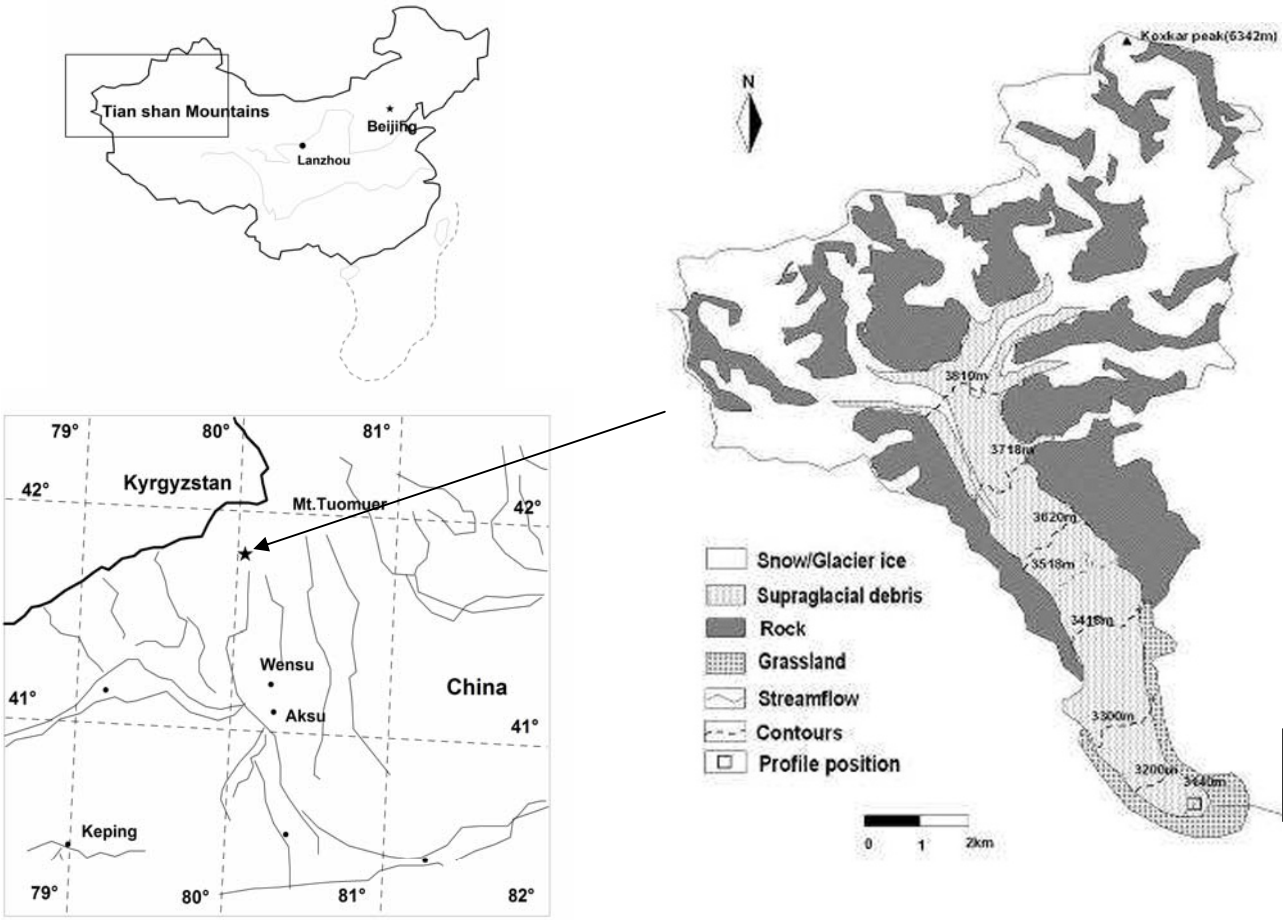

Fig.1. Location and schematic presentation of the Koxkar Glacier.

average thickness of 1.5 m at the toe of the glacier and being more than 2 m thick in some areas (Hai et al. 2006).

We used an SSI (Sensor Software Inc., Canada) Pulse EKKO-PRO GPR with different antennas working at 50, 100 and 200 MHz to detect the same debris section in the thicker part of the debris-covered area of the Koxkar Glacier in June 2008 (a past investigation suggests the debris thickness is around 1–2 m; Fig.1). GPR profiles of both the debris and some of the underlying ice were obtained. The GPR was run in a custom offset mode and traces were artificially triggered. GPR units were towed manually, with antennas mounted on a wooden frame to avoid interference with nearby metal objects. The different antennas were driven along the same tracks, with same starting and stopping points. The transmitting–receiving antennae of three surveys (50, 100 and 200 MHz) were arranged parallel to each other and separated 2 m, 1 m, and 1 m respectively and transverse to the profile direction, and the antenna step distance was 0.1 m to ensure adequate horizontal resolution. The time windows of the profiles were 160, 160 and 140 ns respectively. The accuracy of the radio wave velocity estimate could be improved with 100 and 200 MHz antennas using field methods such as the common midpoint and wide-angle reflection methods. Meanwhile, the survey tracks were recorded with a high-precision GPS.

RESULTS

CMP Velocity Comparison

Precise knowledge of the radar velocity is important in mapping object depth, and the wave velocity relates directly to the media type or permittivity. Because the wave velocity continually changes in a mixed medium, the average wave velocity with regards to a CMP (Mayne, 1962) is generally obtained in detecting an object with a complicated medium on the surface or in the subsurface. Table 1 presents the radar wave velocity for different media. As other media have been well determined, this survey focused on determining related media in the debris layer; Table 1 includes the radar wave velocities of possible media in glacial areas.

In this study, CMP measurements are carried out separately with 100 MHz and 200 MHz antennas. We see from the original 200 MHz CMP data (Fig.2a) that there are almost no reflections after 110 ns, indicating 110 ns (3.2 m) is probably the maximum penetration depth of the 200 MHz antenna. The velocity superposition is relatively concentrated (0.06 m/ns) and the CMP results in Fig. 2b correspond to a time window of about 45 ns (1.5 m). Because the thickness of the debris layer is less than 1.5 m, we conclude that the medium permittivity is relatively evenly distributed in the shallow debris layer, and the subsurface layer has better consistency in each penetration position. The reflected wave signal in Fig. 2c is more powerful than that in Fig. 2a because the wavelength of the 100 MHz antenna is much longer and the energy attenuation much lower. Figure 2d shows that the maximum superposition density is 0.06 m/ns, and the corresponding time window is 110 ns; i.e., the superposition is more dispersed for the 100 MHz CMP result. Furthermore, in the 200 MHz CMP result, the radar wave velocity slightly differs at different positions of the debris layer, and the medium heterogeneity is below the debris layer, so the average wave velocity of the debris layer is 0.06 m/ns. Compared with the debris layer, the medium of the ice body is more uniform and has lower permittivity, but the average velocities for 100 and 200 MHz at different depths are not significantly different, which indicates that there is a medium with higher permittivity in the ice body under the debris layer, which is very likely meltwater.

Table 1. Relative permittivity and velocities as cited in the literature together with the properties we calculate for the USL and ice at Uværsøyra

Medium type	Relative permittivity	Velocity (m/ns)	Source
Ice	3-4	0.150-0.173	Daniels (1996)
Glacier ice	3.1-3.2	0.167-0.170	Eisen et al. (2006)
Snow	1.5-2	0.212-0.245	Eisen et al. (2002)
Soil sandy dry	4-6	0.122-0.150	Daniels (2004)
Soil sandy wet	15-30	0.055-0.077	Daniels (2004)
Soil loamy dry	4-6	0.122-0.150	Daniels (2004)
Soil loamy wet	10-20	0.067-0.095	Daniels (2004)
Sand saturated	10-30	0.055-0.095	Daniels (2004)
Sand dry	4-6	0.122-0.150	Daniels(2004)
Permafrost	4-8	0.106-0.150	Daniels (2004)
Rock	5-8	0.10-0.150	Brandt et al. (2007)
Debris	12-30	0.05-0.070	This study
Ice under debris	3-4	0.15-0.170	This study
Hardpan	4-7	0.157-0.170	This study

Polarity and Amplitude Comparison

When passing through two different medium interfaces, a radar wave returns three half-cycle wavelets (Arcone, Lawson et al. 1995). The expression of 'in debris layer region of a glacier lead to corresponding changes in amplitude, and the change in the waveform phase is mostly described by the reflection coefficient r.

$$r = \frac{\sqrt{\varepsilon_1} - \sqrt{\varepsilon_2}}{\sqrt{\varepsilon_1} + \sqrt{\varepsilon_2}} \quad (1)$$

Here, ε_1 and ε_2 are the dielectric constants of two different media. The greater the contrast between the two

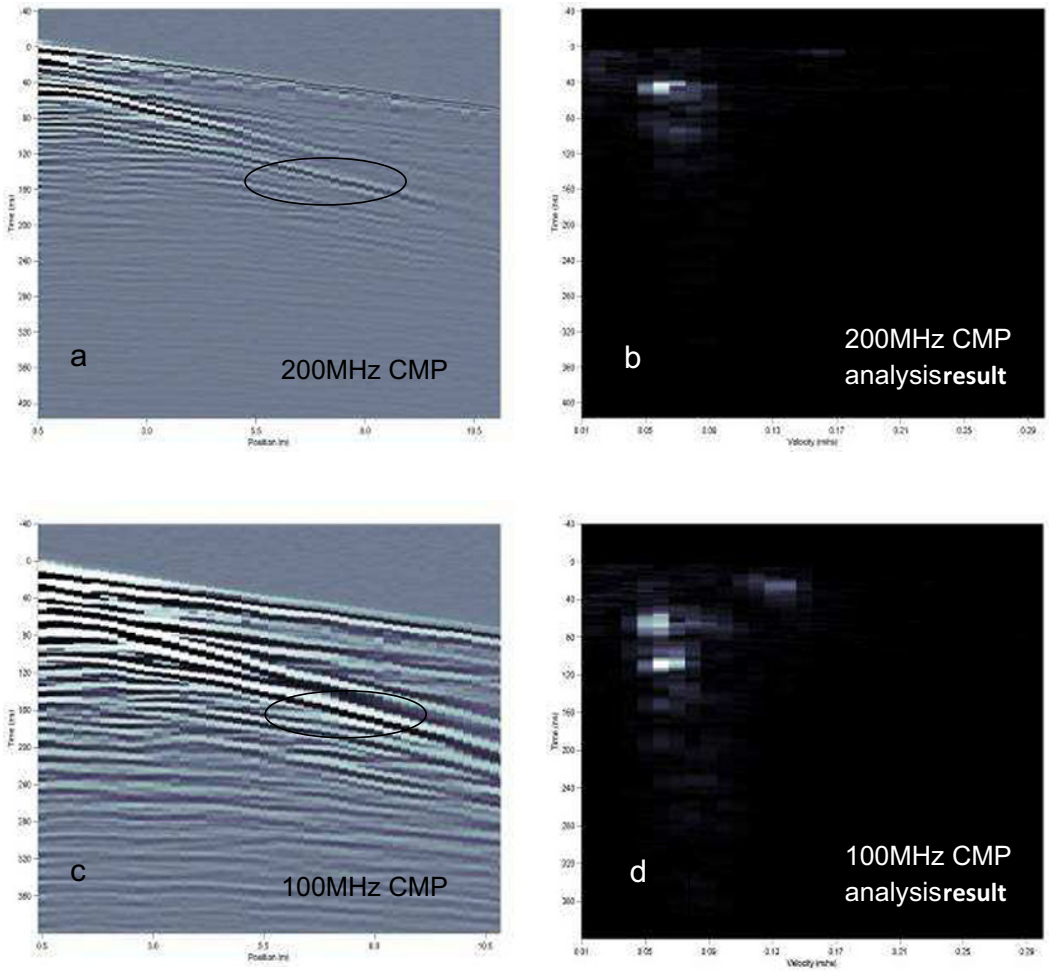

Fig.2. Original CMP image and analytical results for 100 and 200 MHz; original 200 MHz CMP image **(a)**, 200 MHz CMP analysis result **(b)**, original 100 MHz CMP image **(c)**, and 100 MHz analysis result **(d)**.

dielectric constants, the greater the absolute value of the reflection coefficient r.

Figure 3 shows three continuous radar traces obtained from 50 MHz data. The waveforms in the case of continuous interface have reflections described by a negative–positive–negative pulse, and the fluctuation in the amplitude decreases after the pulse, which indicates that r is a maximum at 50 ns and that the dielectric constant of the lower medium is less than that of the upper medium. Comparing the dielectric constant of debris (ε = 12) with that of the ice body (ε = 3),

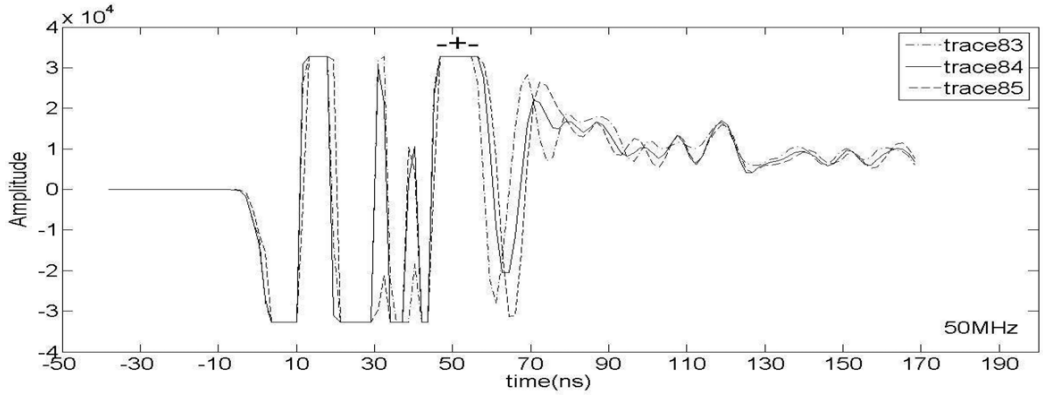

Fig.3. Waveform of three continuous radar traces obtained from 50 MHz data.

we note that when the radar passes through the debris to the ice body, there is a negative–positive–negative pulse reflection. Therefore, the continuous interface in Fig.3 should be the interface between the debris layer and the underlying ice.

DEBRIS AND SUB-GLACIAL STRUCTURE

Theoretical resolutions of GPR in materials commonly found in the glacial and periglacial environment; the theoretical limit for resolving the layer thickness is between 1/4 and 1/2 of the wavelength (Bernabini et al. 1995; Smith and Jol, 1995),

Figure 4 presents the results obtained using the 50, 100 and 200 MHz antennas for the same cross-section. There are significant differences in the three images owing to the different number of superimposition sample points and differences in vertical resolution and energy degradation.

The reflection marked as position 2 in Fig. 4c has a number of hyperbolic diffractions in the supraglacial debris from a depth of about 1.5 m to the surface. Compared with the 50 and 100 MHz radar profiles, the 200 MHz profile has obvious reflections near the ground surface, but its echoes are not strong under the supraglacial debris because of the rapid energy degradation characteristics of the high-frequency antenna. The reflection at 50 MHz is more consistent than that at 100 MHz, which indicates the difference in permittivity in the study area. However, at the interface of the supraglacial debris and ice body, the 50 MHz profile has larger amplitude. Compared with the 50 MHz radar profile, the 100 MHz radar profile seems more shattered under the debris and ice interface and presents more radar clutter in the corresponding area. These characteristics support the conclusion of the preceding CMP analysis that the ice body near the debris has a more uneven distribution with increasing depth, which gradually becomes less apparent greater depth.

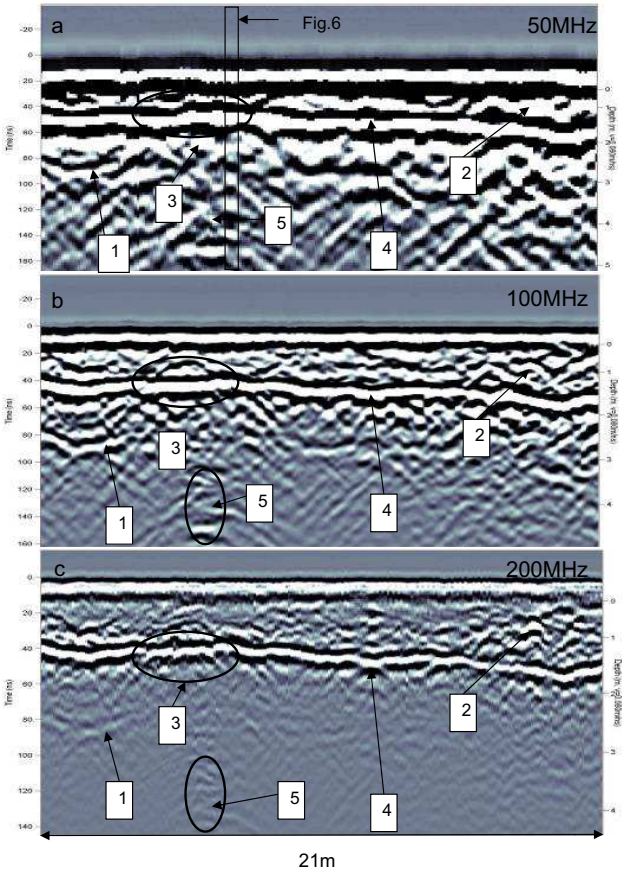

Fig.4. Radar profile of the position marked in Fig.1 obtained at 50, 100 and 200 MHz respectively.

Table 2. The resolution of different media in the use of the different antennas

Material	Propagation velocity	Antenna frequency 50MHz	100 MHz	200 MHz
Cold ice	0.167 m/ns	0.84–1.67 m	0.42–0.84 m	0.21–0.42 m
Temperate ice	0.150 m/ns	0.75–1.50 m	0.38–0.75 m	0.19–0.38 m
Dry rock	0.120 m/ns	0.60–1.20 m	0.30–0.60 m	0.15–0.30 m
Wet rock	0.100 m/ns	0.50–1.00 m	0.25–0.50 m	0.13–0.25 m
Silts	0.070 m/ns	0.35–0.70 m	0.18–0.35 m	0.09–0.18 m
Clay	0.060 m/ns	0.30–0.60 m	0.15–0.30 m	0.08–0.15 m
Fresh/salt water	0.033 m/ns	0.17–0.33 m	0.08–0.17 m	0.04–0.08 m

It is estimated from the waveform analysis that the continuous reflecting layer in Fig. 4 is the interface between debris and underlying ice. It is generally believed that the medium under debris mostly is an ice body with low permittivity. However, there are other strong reflections in the 50 and 100 MHz images, which suggest other mediums in the ice body near the supraglacial debris.

The reflection marked as position 1 in Fig. 4 cannot be well distinguished from the background in image a. Compared with the background, position 1 in image b has a clear reflection outline. The reflection is much weaker in image c owing to the rapid loss and absorption of the high-frequency antenna signals. This suggests that the radar wave has passed through some medium having a high attenuation coefficient, such as silt or wet clay (1–300 dB/m). The electromagnetic wave degradation and absorption through the medium are related to the frequency, as well as the medium's humidity (Daniels 2005; Berard and Maillol 2007). Considering the amplitude analysis of position 1, the medium at position 1 probably has high water content. In the melting season, the ice body under the supraglacial debris probably melts, and the water probably penetrates

downward through cavities and crevasses within the ice body. Some clay and gravel initially present in the debris may be conveyed downward along with the meltwater and later settle in the cavities and crevasses. Therefore, position 1 probably corresponds to the presence of silt or wet clay.

Position 2 is more distinguished from the background in image c than in images a and b, indicating a symmetric hyperbolic point-source reflection, which is hardly even distinguished in image a. Owing to a number of different sized stones in the debris, no great fluctuations in permittivity are determined through polarity analysis. Both signals indicate that rock fragments probably cause hyperbola reflections in the area of the debris and ice body interface. From the antenna resolutions, we conclude that the sizes of rock fragments range from 0.3 to 0.6 m.

Positions 3 and 4 in Fig. 4 show the profile of the interface between the debris-covered layer and the ice body. As seen in the 50 MHz (a) and 100MHz (b) images, the profile is fairly continuous, whereas a fracture is seen to a certain degree in the 200 MHz image. The fine distinctions of the interface are not clearly displayed in images a and b owing to their resolution; however, they can be seen clearly in image c. After careful analysis, we believe that the interfaces of debris and ice in positions 3 and 4 are not continuous, and that the size of the debris or ice body responsible for discontinuity and migration of the interface is less than 0.21 m. There are two possible reasons for the profile fracture. (1) The supraglacial debris is a mixture of rocks of all sizes, and pressing and rubbing between the bottom of the supraglacial debris and top of the ice body is similar to that between the bedrock and the bottom of the glacier. Thus, part of the underlying ice body may rapidly melt under certain pressure and friction, and some of the debris falls downward. Therefore, the mixture is seen to have minor faults in the radar profile. (2) Heat from the debris surface transfers to the ice body, although the thicker supraglacial debris insulates the underlying ice body. In the melting season, the underlying ice body may absorb heat from the debris above, which probably leads to strong melting on a local scale, and some debris falls into the ice body.

Position 5 in Fig. 4 corresponds to reflection at a relatively deep position of the underlying ice body. From the results obtained using the three antennas with different frequencies, it can be confirmed that the radar echoes continue downward from the interface between debris and the ice body. This suggests that the actual reflector is larger, at least 0.84 m, and indicates that there is probably a large melting zone in the ice. As the radar wave passes through the pure ice body, the radar image commonly displays a smooth zone; however, at position 5, minor folds suggest that the ice body contains different impurities. The reflection is continuous from top to bottom; therefore, we believe that the melting water penetrates downward from the interface between the supraglacial debris and ice body. This would lead to ice gradually melting from top to bottom, and thus, the remarkable reflection at position 5 is probably the reflection of sedimentary debris carried by meltwater.

In order to test our interpretation of Position 5 in Fig. 4, we have used a Finite-Difference Time-Domain (FDTD) (Lee, Venkatarayalu et al. 2002; Sneddon and Survey 2002; Moran, Greenfield et al. 2003; Diamanti, Giannopoulos et al. 2008; Guan and Hu, 2008) model that solves Maxwell's equations in two dimensions(Fig.2). Same modeling technique has been used previously by Andrea and others.

The model was run repeatedly to account for different geometries and medias. The input parameters were based on each radar image to be validated. The central frequency was set to 50 MHz and a grid cell size of 0.125 m was used in all simulations. A Ricker wavelet source was used as a rule of thumb. Different scan times were used in simulations for different media. It should be stressed that FDTD simulation focuses on form and identifying medium, rather than scale.

Figure 5 presents three simulation results for vertical void of different form. Figure 5a(1) presents observed and modeled radar images of a crevasse with vertical walls and two small inner bridges. The modeled radar image shows clear superimposed hyperbolic reflections. Which shows the steep incidence angle of the radar signal on the vertical walls causes more energy to be deflected and lost downward and sideways.

There are several superimposed hyperbolic reflections within underlying ice in position 5 in Fig. 4, Comparison with the simulation results, which indicates that the reflections are caused by adjacent englacial void. According to the variation distance described above, it can be concluded that void widths show irrigular distribution form top to bottom.

DISCUSSION

Multi-frequency Antenna

Radar profiles obtained using three antennas with different frequencies clearly show the interface of the supraglacial debris and underlying ice body. The degradation and absorption of electromagnetic waves through a medium depend on the frequency of the waves as well as the medium humidity. When the medium has a greater water content, the electromagnetic wave degradation is

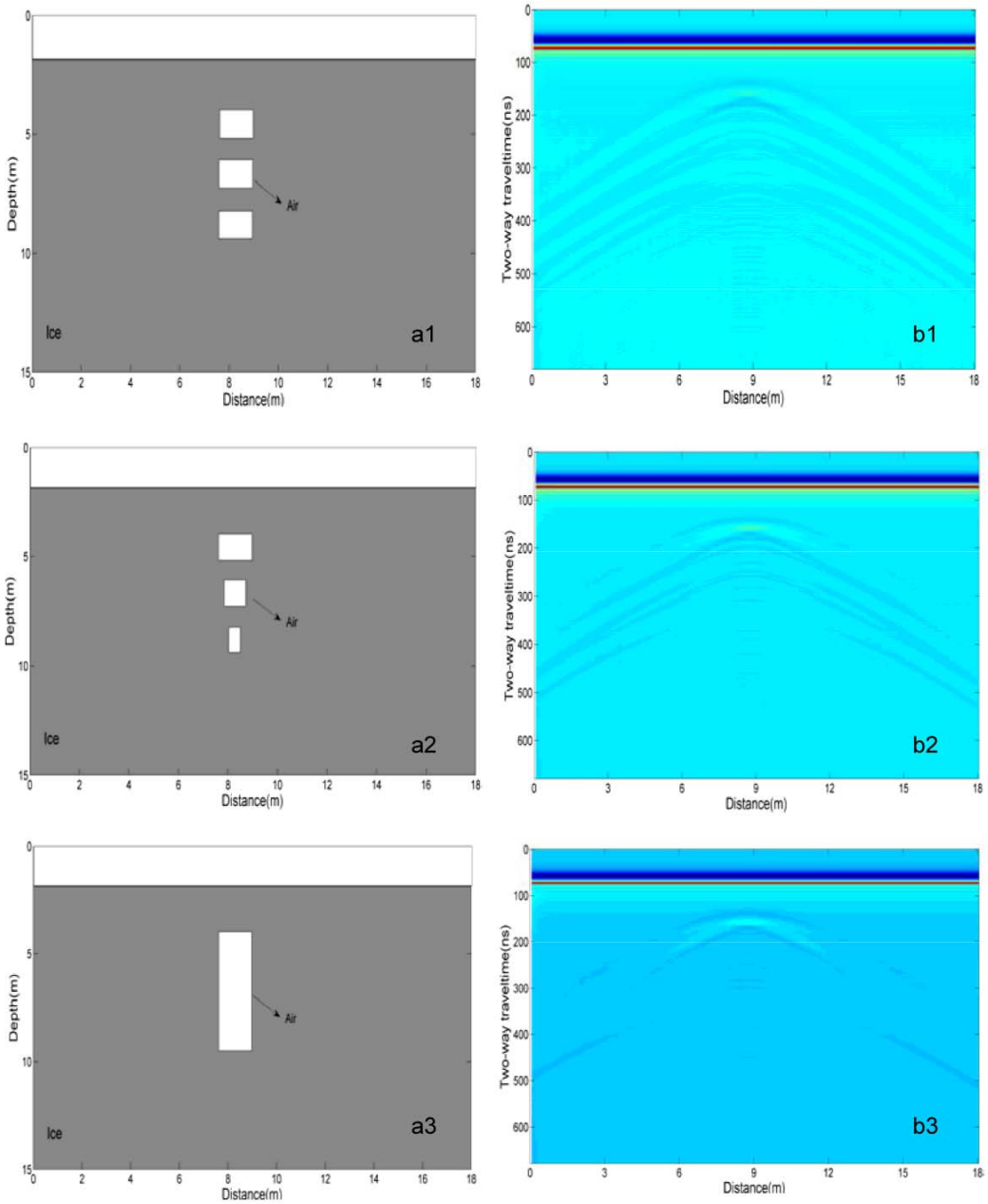

Fig.5. Modeling of continuous square crevasses. Modeled geometry (continuous same square crevasses), a(1); modeled geometry (continuous difference square crevasses), a(2); modeled geometry (long square crevasses), a(3); modeled radar image, b(1,2,3).

quicker (Baili et al. 2009), especially at high frequency. Therefore, we can estimate the water content in different profile positions through degradation features. In an experiment, we find that the ideal penetration depths in terms of resolution for 50, 100, and 200 MHz antennas in a debris-covered area are 150 ns (4.5 m), 100 ns (3 m) and 60 ns (1.8 m) respectively, and that the 100 MHz antenna performs fairly well for an ice body near debris, while the 200 MHz antenna is better for the supraglacial debris.

The resolution of GPR is directly related to the antenna (Bano et al. 2000; Brosten et al. 2006; Booth et al. 2009; Bradford et al. 2009). Figure 6 presents the average amplitudes of the three antennas with different frequencies. The 50 MHz antenna provides the largest average amplitude and the worst resolution comparing with the 100 MHz and 200 MHz antennas, whereas the 200 MHz antenna provides the smallest average amplitude and the best resolution, especially near the surface at 0-1.5 m. The higher the frequency, the less the maximum penetration depth, When penetrating a medium of crushed stone and loose pebble,

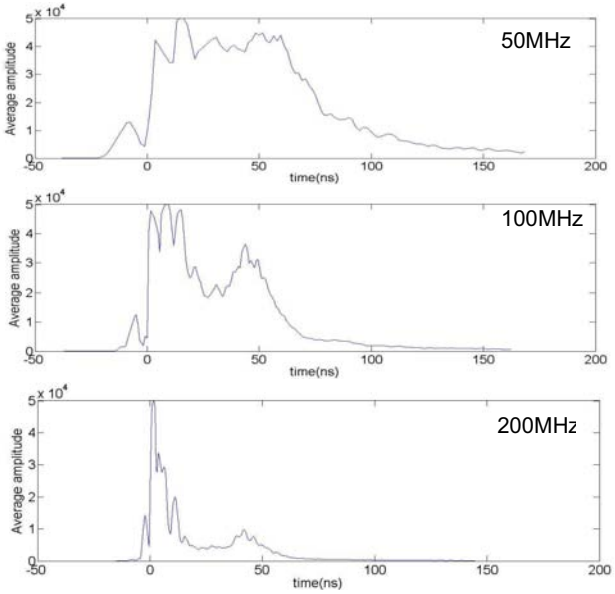

Fig.6. Average amplitudes of 50, 100 and 200 MHz antennas in the Fig. 3 profile.

the maximum depth in the case of 50 MHz is 47 m and the maximum depth in the case of 200 MHz is 28 m (Jol 1995), while the resolution in the case of 50 MHz is 0.6–1.2 m and that in the case of 200 MHz is 0.15–0.3 m. That is, in the detection of debris at varying depth and with varying surface characteristics, more information can be acquired by repeat measurements with antennas having different frequencies.

Debris Thickness and Distribution of Englacial Melting Water

From analysis of the radar wave in terms of polarity and amplitude, it is found that there is always local ablation at the interface between debris and the underlying ice body and within the ice body. The horizontal continuity in the image indicates that the layered distribution in the debris-covered area of the glacier is regular. However, obvious reflections in the underlying ice suggest that there is some filler having high water content within the ice (such as mud or silt). In addition, empty cavities in the underlying ice are also identified (position 5 in Fig.4), which shows the debris thickness have great effect for underlying ice ablation..

Figure 7 presents a map of englacial intense ablation and the distribution of debris thickness According to the results for the englacial structure and debris thickness (Fig.7), the position of englacial intense ablation mainly distributed in the location of thinner debris. It is concluded that the position of the most intense ablation at the glacial surface is not at lower altitude terminus definitely, For such a glacier covered by thick debris, ice body in a glacier covered by thin debris is affected by temperature, on the contrary, the

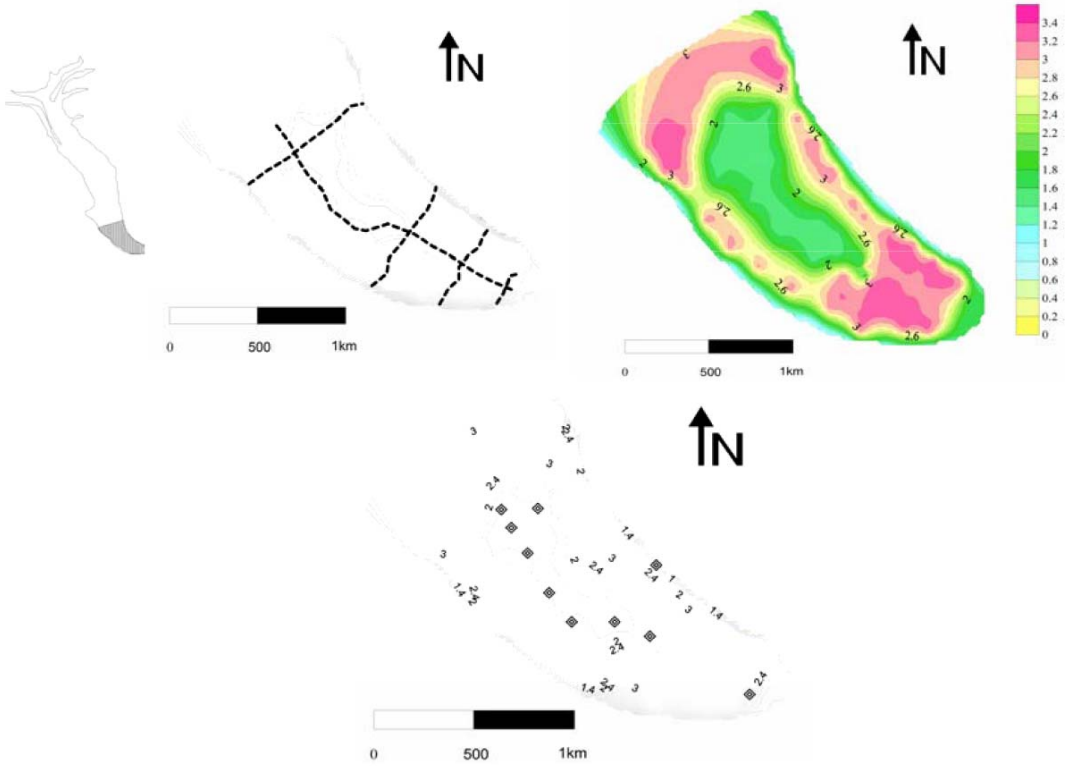

Fig.7. The track of GPR survey line (a), the position of englacial intense ablation (b), the distribution of debris thickness (c).

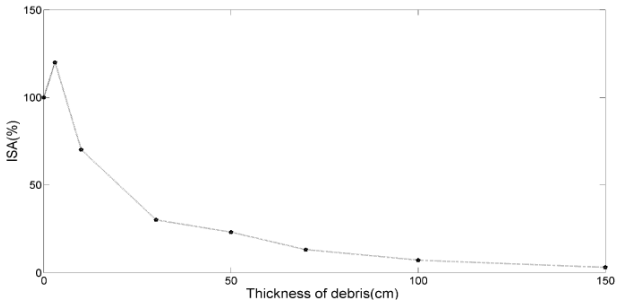

Fig.8. The relation of Intensity of surface ablation (ISA) under debris of diûerent thickness.

one by thick debris is seldom affected by temperature, but it is affected by englacial ablation.

Figure 7 presents the relation of intensity of surface ablation and debris thickness, which shows when surface debris thickness is more than 3 cm it acts as an insulator against external temperature variations on the ice body, Our survey shows that the thickness of debris at the terminus of 3100 to 3300 m a.s.l is far greater than 3 cm(Han et al. 2010).

The Effect of a Debris Layer on Ablation of Glacier Ice

In different positions of the same glacier, the debris thickness distribution is affected by many factors. Debris thickness tends to increase as the elevation of the Koxkar Glacier decreases. The topography, microclimate, and ice-layer ablation under debris also affect the debris thickness at the same altitude. The structure and water content determine the debris thickness to a certain extent. The debris that the main components are dry sand or rock have a great thermal conductivity (Fig. 9) and the debris that the main components are clay and silt will protect the underlying ice from external radiation these kind of debris mainly distributed in glacier terminus.

Based on (SPOT) image (5m resolution)taken in late April 2006, Han et al discribed the distribution of the ice cliffs and supraglacial ponds (Han et al. 2010) ,this study shows that there is intense supraglacial ablation between 3300 and 3700 m. The shrinkage of the Koxkar glacier terminus was less than 2% of the total length during the period 1988-2006(Changwei et al. 2007).

According to the results for the distribution of the ice cliffs and supraglacial ponds, it is concluded that the position of the most intense ablation at the glacial surface is not at the terminus but at higher altitude, where the glacier is covered thinly with debris and affected greatly by temperature. This intense ablation at high elevations leads to accumulation of melt water at the surface, which forms glacial surface lakes and accelerates their expansion. At the same time, the rugged glacial surface and thick debris cover results in much of the discharge of the surface lake draining through englacial streams rather than surface rivers. With the expansion of glacial surface lakes, lake water transfers heat to adjacent ice, thus contributing to the warming of the ice body in these regions. This drainage promotes the development of subglacial water systems and thus the melting and thinning of ice in some regions and thinning of the glacier. In the context of climate warming, the expansion of glacial surface lakes and intensification of englacial melt are mutually promoting.

The rate of glacier thinning will therefore increase in some regions, and the debris thickness at the terminus will increase in the future, which will further increase the difference in ice thickness between high-altitude areas and the terminus. Therefore, the central positions of intense ablation may be disconnected and there will be a dead ice zone at the terminus owing to the insulation of the ice body by debris Fig.10.

CONCLUSION

Using GPR surveys of the Koxkar Glacier, comparative investigation of the debris layer and underlying ice of the Koxkar Glacier using multi-frequency GPR with antennae having different frequencies, and the performance of the

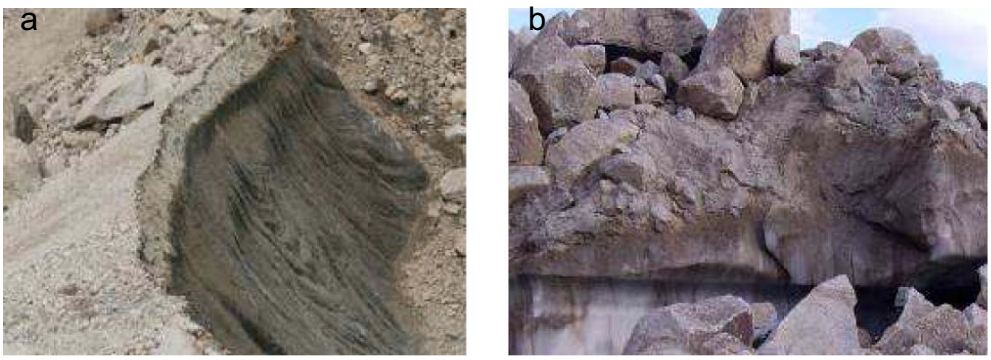

Fig.9. Ice cliff in a debris section of the Koxkar Glacier

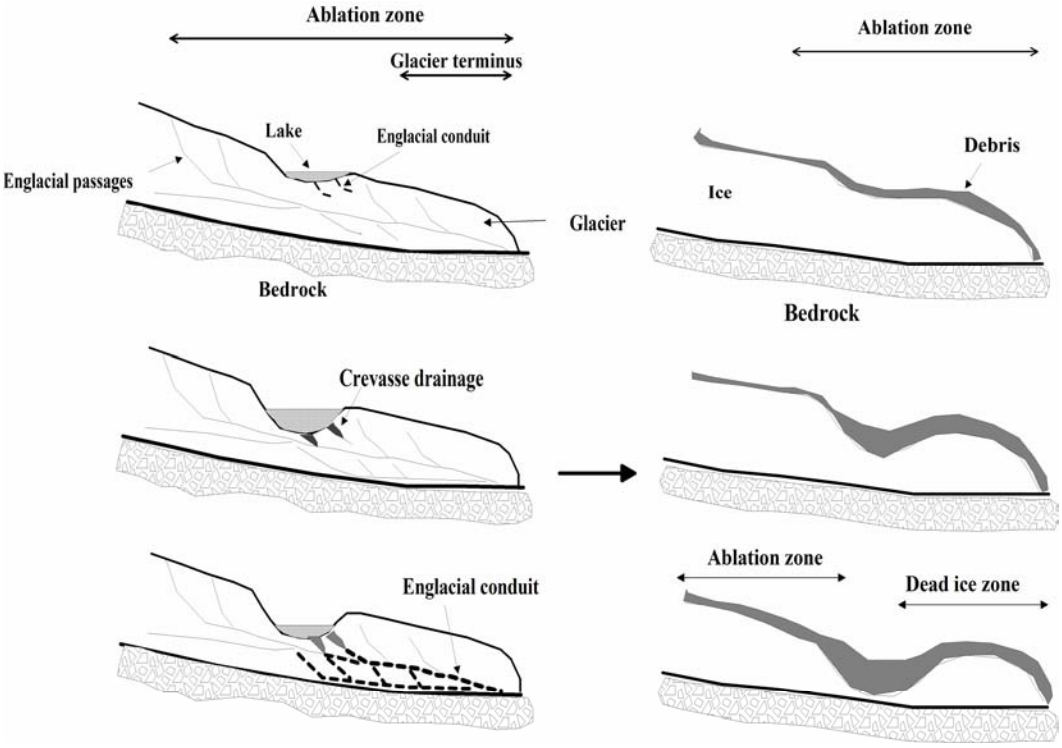

Fig.10. A schematic diagram of the variation of surface lake and terminus in the future.

200 MHz antenna for a debris-covered glacier is best

Due to the effect of debris covered, Local ablation will leads to accumulation of melt water at the surface, which forms glacial surface lakes and accelerates their expansion. At the same time, the rugged glacial surface and thick debris cover results in much of the discharge of the surface lake draining through englacial streams rather than surface rivers, which will affect the glacial ablation way in some extent.

This study, through a combination of GPR survey results and consideration of the characteristics of the glacier itself, reasonably explains these observations, which also shows that some continental glacier will occurs more substantial retreat in the future in the context of climate change. In addition, this study provides a reference for research into the formation mechanisms of the dead ice zone at the terminus of other glaciers. This study provides a reference for research into the formation mechanisms and estimation of the ice volume of glaciers covered by debris.

Acknowledgments: This work was funded by a project of the Tian Shan cryospheric plan (KZCX2-YW-GJ04)The Chinese Glacier Inventory (2006FY110200 and 40601022). We express our thanks to Shang Guandonghui, and Deng Xiaofeng for guidance during the field survey.

References

ADAM, W.G. and KNIGHT, P.G. (2003) Identification of basal layer debris in ice-marginal moraines, Russell Glacier, West Greenland. Quaternary Sci. Rev., v.22(14), pp.1407-1414.

ARCONE, S.A. (1995) Numerical studies of the radiation patterns of resistively loaded dipoles. Jour. Appld. Geophys., v.33(1-3), pp.39-52.

ARCONE, S.A. and LAWSON, D.E. et al. (1995) Short-pulse radar wavelet recovery and resolution of dielectric contrasts within englacial and basal ice of Matanuska Glacier, Alaska, USA. Jour. Glaciology, v.41, pp.68-86.

ARCONE, S.A. and Lawson, D.E. et al. (1998) Ground penetratinng radar reflection profiling of groundwater and bedrock in an area of discontinuous permafrost. Geophysics, v.63, 1573p.

BAILI, J. and LAHOUAR, S. et al. (2009) GPR signal de-noising by discrete wavelet transform. NDT&E Internat., v.42(8), pp.696-703.

BANO, M. and MARQUIS, G. et al. (2000) Investigating alluvial and tectonic features with ground-penetrating radar and analyzing diffractions patterns. Jour. Appld. Geophys. v.43, pp.33-41.

BERARD, B.A. and MAILLOL, J.M. (2007) Multi-offset ground penetrating radar data for improved imaging in areas of lateral complexity—Application at a Native American site. Jour. Appld. Geophys. v.62(2), pp.167-177.

BERNABINI, M. and PETTINELLI, E. et al. (1995) Field experiments for characterization of GPR antenna and pulse propagation. Jour. Appld. Geophys., v.33(1-3), pp.63-76.

BISHOP, M.P. and SHRODER J.F. Jr et al. (1995) SPOT multispectral analysis for producing supraglacial debris load estimates for Batura glacier, Pakistan. Geocarto Internat., v.10, pp.81-90.

BOLCH, T. and BUCHROITHNER, M.F. et al. (2007) Automated delineation of debris-covered glaciers based on ASTER data.

BOOTH, A.D. and Endres, A.L. et al. (2009) Spectral bandwidth enhancement of GPR profiling data using multiple-frequency compositing. Jour. Appld. Geophys., v.67(1), pp.88-97.

BRADFORD, J.H. and NICHOLS, J. et al. (2009) Continuous profiles of electromagnetic wave velocity and water content in glaciers: an example from Bench Glacier, Alaska, USA. Annals of Glaciology, v.50(51), pp.1-9.

BROSTEN, T.R. and BRADFORD, J. H. et al. (2006) Profiles of temporal thaw depths beneath two arctic stream types using ground penetrating radar. Permafrost and Periglacial Processes, v.17(4), pp.341-355.

BUTEAU, S. and FORTIER, R. et al. (2004) Numerical simulation of the impacts of climate warming on a permafrost mound. Permafrost and Periglacial Processes, v.15(1), pp.41-57.

CHANGWEI, X. and YONGJIAN, D. et al. (2007) Study on the change of Keqikaer Glacier during the last 30 years, Mt. Tuomuer, Western China. Environ. Geol., v.51(7), pp.1165-1170.

CHIARLE, M. and Iannotti, S. et al. (2007) Recent debris flow occurrences associated with glaciers in the Alps. Global and Planetary Change, v.56(1-2), pp.123-136.

CLARK, D.H. et al. (1994) Debris-covered glaciers in the Sierra Nevada, California, and their implications for snowline reconstructions. Quaternary Res., v.41(2), pp.139-153.

DANIELS, D.J. (2005) Ground penetrating radar. Wiley Online Library.

DIAMANTI, N. and GIANNOPOULOS, A. et al. (2008) Numerical modelling and experimental verification of GPR to investigate ring separation in brick masonry arch bridges. NDT & E International, v.41(5), pp.354-363.

EISEN, O. and WILHELMS, F. et al. (2006) Improved method to determine radio-echo sounding reflector depths from ice-core profiles of permittivity and conductivity. Jour. Glaciology, v.52(177), pp.299-310.

GUAN, W. and HU, H. (2008) Finite-difference modeling of the electroseismic logging in a fluid-saturated porous formation. Jour. Computational Physics, v.227(11), pp.5633-5648.

HAIDONG, H. and YONGJING, D. et al. (2006) A simple model to estimate ice ablation under a thick debris layer. Jour. Glaciology, v.52(179), pp.528-536.

HAN, H. and LIU, S. et al. (2010) Glacial runoff characteristics of the Koxkar Glacier, Tuomuer-Khan Tengri Mountain Ranges, China. Environ. Earth Sci., v.61(4), pp.665-674.

HAN, H. and WANG, J. et al. (2010) Backwasting rate on debris-covered Koxkar glacier, Tuomuer mountain, China. Jour. Glaciology, v.56(196), pp.287-296.

HODSON, A.J. and FERGUSON, R.I. (1999) Fluvial suspended sediment transport from cold and warm based glaciers in Svalbard. Earth Surface Processes and Landforms, v.24(11), pp.957-974.

HUBBARD, B.P. and HUBBARD, A. et al. (2003) Spatial variability in the water content and rheology of temperate glaciers: Glacier de Tsanfleuron, Switzerland. Annals of Glacio., v.37(1), pp.1-6.

IRVINE FYNN, T. and MOORMAN, B. et al. (2006) Seasonal changes in ground penetrating radar signature observed at a polythermal glacier, Bylot Island, Canada. Earth Surface Processes and Landforms, v.31(7), pp.892-909.

JOL, H.M. (1995) Ground penetrating radar antennae frequencies and transmitter powers compared for penetration depth, resolution and reflection continuity. Geophysical Prospecting, v.43(5), pp.693-709.

LEE, K.H. and VENKATARAYALU, N. et al. (2002) Numerical modeling development for characterizing complex GPR problems, Society of Photo-Optical Instrumentation Engineers.

MAYNE, W.H. (1962) Common reflection point horizontal data stacking techniques. Geophysics, v.27(6), pp.927.

MIHALCEA, C. and MAYER, C. et al. (2006) Ice ablation and meteorological conditions on the debris-covered area of Baltoro glacier, Karakoram, Pakistan. Annals of Glaciology, v.43(1), pp.292-300.

MOORMAN, B.J. and ROBINSON, S.D. et al. (2003) Imaging periglacial conditions with ground penetrating radar. Permafrost and Periglacial Processes, v.14(4), pp.319-329.

MORAN, M.L. and Greenfield, R.J. et al. (2003) Modeling GPR radiation and reflection characteristics for a complex temperate glacier bed. Geophysics, v.68(2), pp.559.

MURRAY, T. and GOOCH, D.L. et al. (1997) Structures within the surge front at Bakaninbreen, Svalbard, using ground-penetrating radar. Annals of Glaciology, v.24, pp.122-129.

NAKAWO, M. and RANA, B. (1999) Estimate of ablation rate of glacier ice under a supraglacial debris layer. Geografiska Annaler: Series A, Physical Geography, v.81(4), pp.695-701.

NAKAWO, M. and YOUNG, G. J. (1981) Field experiments to determine the effect of a debris layer on ablation of glacier ice. Annals of Glaciology, v.2(1), pp.85-91.

Paul, F. and Huggel, C. et al. (2004) Combining satellite multispectral image data and a digital elevation model for mapping debris-covered glaciers. Remote Sensing of Environment, v.89(4), pp.510-518.

PLEWES, L.A. and HUBBARD, B. (2001) A review of the use of radio-echo sounding in glaciology. Progress in Physical Geography, v.25(2), pp.203.

SMITH, D.G. and JOL, H.M. (1995) Ground penetrating radar: antenna frequencies and maximum probable depths of penetration in Quaternary sediments. Jour. Appld. Geophys., v.33(1-3), pp.93-100.

SNEDDON, K.W. and SURVEY, G. (2002) Modeling GPR data to interpret porosity and DNAPL saturations for calibration of a 3-D multiphase flow simulation, US Dept. of the Interior, US Geological Survey.

STOKES, C. and POPOVNIN, V. et al. (2007). Recent glacier retreat in the Caucasus Mountains, Russia, and associated increase in supraglacial debris cover and supra-/proglacial lake development. Annals of Glaciology, v.46(1), pp.195-203.

SU, Z. and Shi, Y. (2002) Response of monsoonal temperate glaciers to global warming since the Little Ice Age. Quaternary Internat., v.97, pp.123-131.

TAURISANO, A. and TRONSTAD, S. et al. (2006) On the use of ground penetrating radar for detecting and reducing crevasse-hazard in Dronning Maud Land, Antarctica. Cold Regions Science and Technology, v.45(3), pp.166-177.

YAFENG, S. and MAOHUAN, H. et al. (2000). Glaciers and their environments in China–the present, past and future, Beijing: Science Press.

(Received: 29 September 2010; Revised form accepted: 20 March 2012)